Published in "Cell Metabolism 19(3): 527–538, 2014"
which should be cited to refer to this work.

Supplemental Information

Hypoglycemia-Activated GLUT2 Neurons of the Nucleus Tractus Solitarius Stimulate Vagal Activity and Glucagon Secretion

Christophe M. Lamy, Hitomi Sanno, Gwenaël Labouèbe, Alexandre Picard, Christophe Magnan, Jean-Yves Chatton, and Bernard Thorens

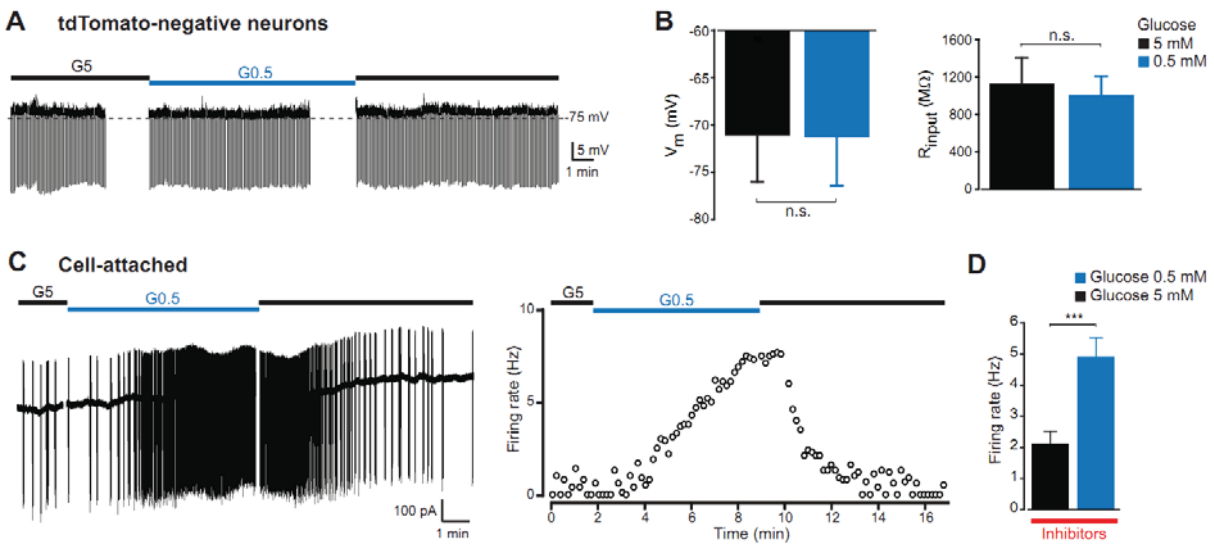

Figure S1. Glucose response of GLUT2 and non-GLUT2 neurons (related to figure 1).

(A) Voltage trace showing the absence of response to glucose concentration change in an NTS tdTomato-negative neuron. G5, glucose 5 mM; G0.5, glucose 0.5 mM.

(B) Bar graphs summarizing glucose effect on V_m and R_{input} on NTS tdTomato-negative neurons (n=5). Data are presented as mean ± SEM; n.s., non significant.

(C) Left, current trace recorded in cell-attached configuration in a NTS tdTomato-positive neuron, and in the presence of synaptic inhibitors showing spontaneous action currents firing in 5mM and 0.5mM glucose. Right, plot of the firing frequency over time in 10 s bins shows an increase in firing under low glucose.

(D) Pooled glucose effects on spontaneous firing frequency in cell-attached configuration in the presence of inhibitors of synaptic transmission confirms the inhibitory effect of glucose on NTS GLUT2 neurons (n=6). Data are presented as mean ± SEM; *** $p<0.001$.

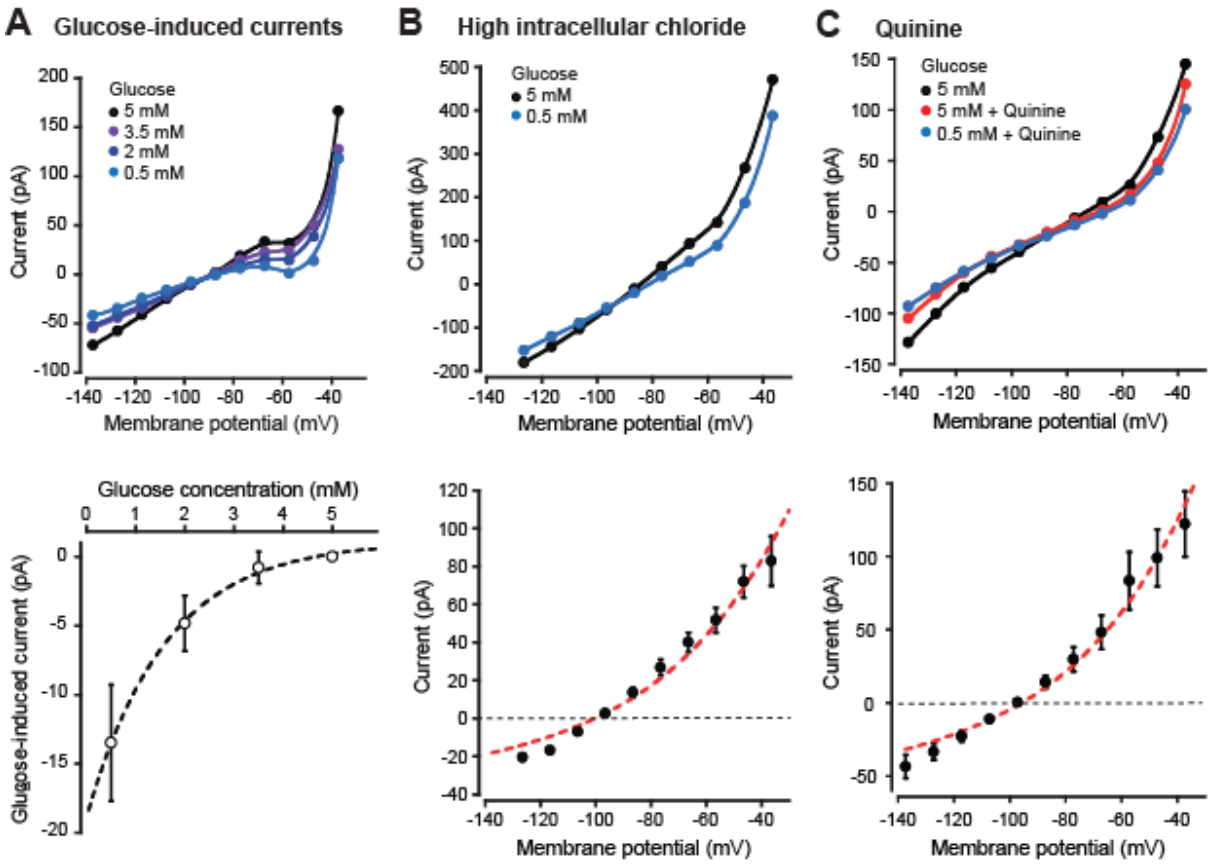

Figure S2. Glucose-induced currents (related to Figure 2).

(A) Top, representative current-voltage plots for graded glucose concentrations between 0.5 mM and 5 mM. Bottom, plot showing the concentration-dependence of net glucose currents measured at -70 mV relative to 5 mM glucose (n=5). Data are presented as mean ± SEM.

(B) Top, current-voltage plot recorded with a high-chloride pipette solution shows a similar shift when changing glucose concentration as when recording with low intracellular chloride. Bottom, the current-voltage plot of net glucose-induced current obtained with high intracellular chloride is identical to the one recorded with low chloride, showing that the glucose-induced current is independent from this ion (n=10). Data are presented as mean ± SEM. Red dashed line represents the Goldman-Hodgkin-Katz current equation fit to the data.

(C) Top, representative current-voltage plots showing the inhibitory effect of quinine on glucose-induced current. Bottom, the current-voltage plot of net quinine-inhibited current confirms that this drug blocks GLUT2 neurons leak K^+ channels at rest (n=7). Data are presented as mean ± SEM. Red dashed line represents the Goldman-Hodgkin-Katz current equation fit to the data.

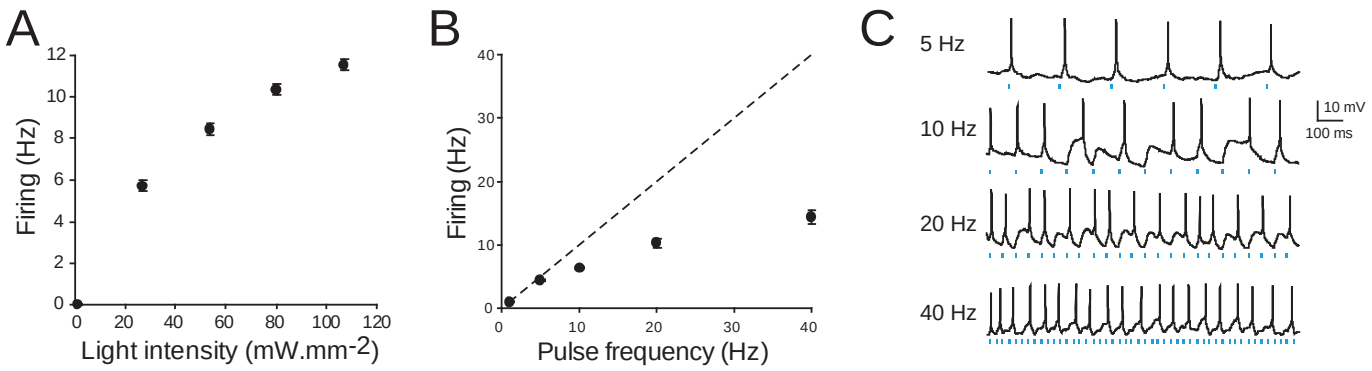

Figure S3. Optogenetic activation of GLUT2 neurons (related to figure 6).

(A) Plot of the average firing rate of GLUT2 neurons stimulated with 400 ms pulses of blue light for different illumination intensities.

(B) Plot of the average firing rate of GLUT2 neurons stimulated with brief pulses (10 ms) of blue light for different laser pulse rates.

(C) Example traces of firing response to brief blue light pulses of increasing frequencies.

Table S1. Intrinsic properties of NTS *Glut2*+ neurons (related to figure 1)

Property	*Glut2*+ neurons (n=32)
Passive membrane properties	
Resting membrane potential, mV	–70.2 ± 1.0
Input resistance, MΩ	738.2 ± 88.5
Membrane capacitance, pF	28.5 ± 2.6
Single action potential properties	
Amplitude, mV	66.9 ± 1.6
Duration, ms	2.2 ± 0.2
fast AHP, mV	16.6 ± 1.5
Threshold, mV	–40.3 ± 1.0
Discharge properties	
F-I slope, Hz.pA^{-1}	0.34 ± 0.04
Accommodation index	0.59 ± 0.05

Values are means ± s.e.m. AHP, afterhyperpolarization; F-I, frequency-intensity curve.

Table S2. Glucose effect on action potential properties (related to figure 1)

Property	Glucose 5 mM (n=12)	Glucose 0.5 mM (n=12)
Single action potential properties		
Threshold, mV	–39.8 ± 2.1	–38.4 ± 2.0
Amplitude, mV	71.0 ± 2.3	70.4 ± 2.7
Duration, ms	2.3 ± 0.3	2.3 ± 0.2
fast AHP amplitude, mV	14.5 ± 2.9	14.9 ± 3.0
fast AHP FWHM, ms	8.3 ± 1.6	8.4 ± 1.5
Discharge properties		
Accommodation index	0.59 ± 0.06	0.63 ± 0.06

Values are means ± s.e.m. AHP, afterhyperpolarization; FWHM, full width at half maximum. Significance: comparison between columns with 2-tailed paired t-tests did not find any significant difference.

Supplemental Experimental Procedures

Slice preparation

All experimental procedures were carried out according to the Ordinance on Animal Experimentation and approved by the veterinary office of Canton de Vaud. *Glut2*-Cre mice (Mounien et al., 2010) were crossed with Rosa26tdTomato reporter mice (Ai9 strain) (Madisen et al., 2010). Offsprings (P14-P23) were anesthetized with pentobarbital and decapitated. Sagittal slices of brainstem, 200 μm thick, containing NTS were cut in ice-cold extracellular solution with 10 mM glucose using a vibratome (VT1000, Leica Microsystems, Heerbrugg). Slices were subsequently maintained in an incubation chamber filled with the slicing extracellular solution at room temperature (22–24°C) and used between 1h and 8h after sectioning.

Electrophysiology

Experiments were done on an LSM510 Meta confocal microscope (Carl Zeiss, Feldbach, Switzerland) mounted on an upright Axioskop FS2 Plus stand and equipped with a motorized stage and micromanipulators (Luigs and Neumann, Ratingen, Germany) controlled by computer software (kindly provided by Rodrigo Perin and Henri Markram, Laboratory of Neural Microcircuitry, EPFL, Lausanne).

Slices were placed in a submerged-type recording chamber (volume ~ 2 ml) and continuously superfused at a flow rate of 2 ml/min with extracellular solution at room temperature (22–24°C). NTS boundaries were set under a low-power objective with infrared differential interference contrast illumination. A 40x/0.8 water dipping objective was then used to localize tdTomato-expressing neurons with confocal epifluorescence microscopy.

Borosilicate glass pipettes with tip resistances ranging from 4 to 5 MΩ where used to obtain whole-cell recordings from visually identified neurons. Recordings were performed with a Multiclamp 700B amplifier (Molecular Devices). Bridge balance and pipette capacitance were adjusted. Signals were low-pass filtered at 3 KHz, sampled at 10 KHz with a Digidata 1440 A/D interface (Molecular Devices), and acquired with pClamp 10 software package (Molecular devices). Cells were held at -70 mV in voltage clamp and with no bias current injection in current-clamp. Cells for which access resistance was above 30 MΩ or changed by more than 20% during the recording were discarded. A settling time of ≥ 10 min was observed after break-through before starting measurements. Continuous recordings of membrane potential were used to monitor the effect of glucose and of metabolically-active drugs. Recordings where resting membrane potential was not stable over time or where the effect of glucose concentration change on resting membrane potential was not reversible were excluded from further analysis. Hyperpolarizing current pulses were periodically injected to monitor

input resistance. The continuous recording was paused when the effect of each experimental condition had reached a plateau to carry out additional measurements of passive and active membrane properties.

Cell attached recordings were performed on slice superfused with a modified extracellular solution to favor spontaneous firing (Dani et al., 2005) with patch pipettes filled with extracellular solution. Action current firing frequency was measured in voltage-clamp mode with a command voltage leading to a holding current of 0 pA.

Solutions and drugs

The standard extracellular solution contained (mM): 125 NaCl, 2.5 KCl, 26 $NaHCO_3$, 1.25 NaH_2PO_4, 2 $CaCl_2$, 1 $MgCl_2$ and 5 D-glucose. Modified extracellular solution used for cell-attached recording contained (mM): 126 NaCl, 3.5 KCl, 25 $NaHCO_3$, 1 NaH_2PO_4, 1 $CaCl_2$, 0.5 $MgCl_2$ and 5 D-glucose. Extracellular solutions made with lower glucose concentrations had sucrose added to compensate for the change in osmolarity.

Whole-cell recordings were done with a pipette solution containing (mM): 130 K-gluconate, 2 NaCl, 1 $MgCl_2$, 10 Hepes, 0.1 EGTA, 10 sodium phosphocreatine, 4 MgATP, 0.5 Na_2GTP. Where mentioned, a high-chloride pipette solution was used and contained (mM): 130 KCl, 15 K-gluconate, 2 NaCl, 1 $MgCl_2$, 10 Hepes, 0.1 EGTA, 10 sodium phosphocreatine, 4 MgATP, 0.5 Na_2GTP. In recordings performed to check the dependency of glucose-induced effect on intracellular glucose processing, 3 mM of glucose was added to the standard pipette solution. We established that this concentration was sufficient to saturate intracellular glucose metabolism while enabling the effect of competitive glucokinase inhibitor D-glucosamine. Biocytin (0.5% w/v) was added to the pipette solution in the cases where we wanted to trace axonal projections with immunohistochemistry. All pipette solutions were adjusted to pH 7.3 with KOH.

In experiments where we wanted to block network-dependent effects, we added the following synaptic blockers to the extracellular solution: 6-cyano-7-nitroquinoxaline-2,3-dione (CNQX, 20 µM, AMPA glutamate receptor antagonist), D-aminophosphonovalerate (D-AP5, 50 µM, NMDA glutamate receptor antagonist), bicuculline (20 µM, $GABA_A$ receptor antagonist), strychnine hydrochloride (1 µM, glycine receptor antagonist). During continuous recordings of glucose-induced currents we blocked network activity by adding tetrodotoxin citrate (TTX, 1 µM, voltage-gated sodium channel antagonsist). In addition, the following drugs were added to the extracellular solution were mentioned: Quinine (200 µM, leak potassium channel blocker), 2-deoxyglucose (2-DG, 10 mM, metabolic inhibitor), D-glucosamine (10-20 mM, competitive inhibitor of glucokinase), Oligomycin (12 µM, inhibitor of

mitochondrial ATPase), 5-amino-4-imidazolecarboxamide riboside (AICAR 500 μM, AMPK allosteric activator), Compound C (150 μM, AMPK inhibitor).

CNQX, D-AP5 and bicuculline were from Ascent Scientific (Cambridge, UK). TTX was from Biotrend (Anawa, Wangen, Switzerland). Strychnine hydrochloride, quinine hydrochloride, AICAR and compound C were from Tocris Bioscience (R&D Systems Europe, Abingdon, UK). Oligomycine, D-glucosamine and 2-deoxyglucose were from Sigma (Sigma-Aldrich, Buchs, Switzerland).

Data analysis

Electrophysiological data were analyzed with pClamp 10 (Molecular Devices). Data were corrected for calculated liquid junction potentials. Input resistance was monitored in current-clamp mode by periodic by 500 ms hyperpolarizing current pulses and calculated according to Ohm's law as the ratio of the voltage deflection measured at steady state over the intensity of the current pulse. For cell attached recordings, action currents were detected by template matching and firing rate was subsequently calculated over 10 s bins. Values of resting membrane potential, input resistance and firing rate obtained from continuous traces were plotted over time in Excel (Microsoft) and effects of glucose and drugs on these parameters were measured as averages over 1 min at the plateau of effect.

Current–voltage relationships (IV curves) were obtained by measuring steady state currents during successive hyperpolarizing and depolarizing voltage steps from the holding potential. Net glucose current IV curves, obtained by subtracting current values measured at 0.5 mM glucose from those measured at 5 mM glucose, were fitted by the Goldman-Hodgkin-Katz current equation (Hille, 2001).

Frequency-intensity curves (FI curves) were established by measuring the discharge frequency for depolarizing current steps of increasing intensities. The gain of FI curve was computed as the slope of the fit to the linear part of the FI curve. The rheobase was measured as the current intensity eliciting the first action potential during a slowly rising current ramp.

Single action potential (AP) properties were measured on the first AP elicited by near-threshold depolarizations. The AP threshold was calculated as the membrane potential at which its first derivative reached 10 mV ms^{-1}. AP duration was the time for membrane potential to return to the threshold value. Amplitudes of the AP and of the fast afterhyperpolarization (fast AHP) were determined from threshold. The discharge response to a 2 s current step was used to establish the firing pattern. The accommodation index was quantified as the ratio between the first and the last interspike intervals during the discharge response.

Group data were presented as averages ± s.e.m. Statistical inference testing was performed with paired and unpaired 2-tailed Student's t tests. Differences were considered significant for $p < 0.05$. Statistical analysis and curve fitting were done with Origin 8.5 (OriginLab).

Single cell RT-PCR

For single-cell transcripts amplification, RNAse-free pipette solution and patch pipettes were prepared. The silver wire was rechlorinated just before the experiment. Whole-cell configuration was established. At the end of the recording, the cytosol was slowly aspirated under visual control by applying gentle negative pressure to the pipette. Negative pressure was removed and the pipette was carefully withdrawn to avoid contamination.

The aspirated single-cell content was expelled into the RNase free PCR tube containing 0.5 μl RNasin (40 U/μl; Promega), 1 μL random primer (0.5 μg/μl; Invitrogen), and 0.5 μl of 20 mM dNTPs. It was incubated at 70 °C for 5 min and 4 °C for 10 min. Then 4 μl of 5x First Strand Buffer (Invitrogen), 1 μl of 0.1 M DTT, 0.5 μl of RNasin, and 0.5 μl of Reverse Transcriptase superscript II (200U/μl; Invitrogen) were added for reverse transcription and incubated at 37 °C for 60 min. This was followed by heat inactivation at 70 °C for 10 min and incubation at 4 °C for 10 min.

The PCR conditions were optimized for each gene. We performed two successive PCR rounds. The first round of PCR used the cDNAs present in the reverse transcription reaction as a template, complemented with 2 μl of each 10 μM primers, 1 μl of 20 mM dNTPs, 1 μl of HotStart Taq plus DNA polymerase (5 U/μl; Qiagen) in a final volume of 50 μl. For the second round of PCR, 10 μl of the first PCR product were used as template with addition of 0.4 μl of each 10 μM primers, 0.4 μl of 20 mM dNTPs, and 0.1 μl of KAPA 2G Fast DNA polymerase (5 U/μl; KAPA Biosystems) final volume of 20 μl. The products of the second PCR product were analyzed in agarose gel using ethidium bromide.

PCR primers used for *Glut2* were : forward 5'-TGC TTC CAG TAC ATT GCG GA-3' and reverse 5'-TGA TAT TTC TAA TCG GAG TC-3' (amplicon size 364 bp) and for beta actin: forward 5'-GCC AAC CGT GAA AAG ATG AC-3' and 5'-GCA CTG TGT TGG CAT AGA GG3'(amplicon size 560 bp).

Immunohistochemistry

To study the co-localization of GLUT2 with neuronal markers GAD67 and parvalbumin (PV), pAMPKα *Glut2*-Cre/tdTomato mice were perfused with 4% paraformaldehyde. The brains were removed, postfixed,cryoprotected for 24 h and frozen on dry ice. Cryosections from brainstem (25 μm) were

prepared. Sections were washed with PBS, blocked with 0.1 % TritonX-100/10% NGS in PBS 3 h and incubated with primary antibodies against GAD67 (MAB5406, Chemicon, Temecula, CA, USA, 1:500), PV (PV235, Swant, Bellinzona, Switzerland, 1:1000) or pAMPKα (ab2535, Cell Signalling Technology, Danvers, MA, 1:200) in 0.1% TritonX-100/3% NGS/PBS overnight. They were then incubated with a FITC-coupled secondary antibody diluted 1:100 in 3% NGS/PBS for 3 h, washed, mounted on glass slides and coverslipped with Vectashield (Vector H-1000) mounting medium.

To investigate the interaction of NTS GLUT2 neurons with DMNX cells, we filled tdT+ neurons during whole-cell recording with a pipette solution containing 0.5% (w/v) biocytin for ≥ 20 min to allow the marker to diffuse to distal cell processes. After recording, slices were fixed with PFA 4% at +4°C overnight. A set a slices with no biocytin-filled cells were also processed. All slices were rinsed with PBS, incubated in a permeabilizing solution containing 10% NGS and 0.5% triton X-100 for 5h in PBS at room temperature and transferred to PBS containing a mouse monoclonal antibody against choline acetyltransferase (ab35948, Abcam, 1:300) at +4°C for 3 days. After further rinsing in PBS, slices were incubated in PBS containing an anti-mouse antibody coupled to AlexaFluor647 (A21235, Invitrogen, 1:200) and Cascade Blue-Neutravidin (A2663, Invitrogen, 1:100) overnight. After final rinsing, slices were mounted on glass slides and coverslipped with Vectashield (Vector H-1000) mounting medium.

Image acquisition and processing

Confocal images of immunostained cryosections were taken on a LSM 510 Meta confocal microscope with a 40x1.3 N.A. oil immersion objective (Carl Zeiss, Feldbach, Switzerland), with the appropriate excitation beams and filter sets. Stacks were acquired (512x512 pixels, 4 times averaging) with a step size of 0.6 mm and processed with Image J (Rasband, W.S., NIH, Bethesda, Maryland, USA, http://imagej.nih.gov/ij/) to obtain maximum intensity projection representations. The absence of cross-talk between imaging channels was checked by acquiring separate image sets for each of the excitation beams individually.

Confocal images of recorded slices were taken on a LSM 710 Quasar confocal microscope (Carl Zeiss, Feldbach, Switzerland). A 20x0.5 N.A. dry objective was used to acquire juxtaposed stacks covering the whole dorsal vagal complex area to visualize the recorded cell and it axonal projections. Further images were taken with a 63x/1.4 N.A. oil immersion objective to get high resolution stacks (1024x1024, 4 times averaging, 0.2 mm z step size) of biocytin-filed axonal projections in DMNX. These images were 3D reconstructed and represented as maximum intensity projections with Imaris image analysis software (Bitplane, Zurich, Switzerland).

Optogenetics experiments

Glut2-Cre mice (Mounien et al., 2010) were crossed with Rosa26ChR2-YFP reporter mice (Ai32 strain) (Madisen et al., 2012). Acute brain slices were prepared from offspring (P14-P23) as described above to perform electrophysiological recordings from NTS ChR2-expressing neurons. These cells were targeted thanks to the co-expression of YFP with ChR2 and recorded by whole-cell patch-clamp (see above). Light stimulation was achieved with an optical fiber coupled to a laser source (473 nm, Rapp Optoelectronics, Wedel, Germany) and brought close to the recorded cell with a micromanipulator. Light pulses were triggered by a custom-made electrical stimulus generator controlled by the electrophysiology software (pClamp).

For in vivo experiments, *Glut2*-Cre$^{tg/+}$xChR2$^{tg/+}$ mice and G*lut2-Cre*$^{+/+}$xChR2$^{tg/+}$ littermates were anesthetized with isoflurane and placed on a heating blanket to maintain the body temperature at 37.0 ± 0.2°C. Open access to the caudal brainstem was obtained after dissecting the neck muscles in the midline and removing the tentorium cerebelli. The neck was sharply flexed to enable access to the more rostral portions of the NTS (Berthoud et al., 1990). An optical fiber (200 μm diameter core, NA 0.48) coupled to a laser source (473 nm, Rapp Optoelectronics, Wedel, Germany) was attached to a stereotaxic micromanipulator and positioned above the NTS. The light stimulus was delivered for 40 min with a protocol that was shown to elicit neuronal firing in vitro (10-15 mW, 10 ms pulses at 20 Hz for 1s every 4s). Activity of the vagus nerve was continuously recorded for 10 min before, during and for 10 min after photostimulation as previously described (Magnan et al., 1999). Brieflly, the vagus was exposed along the carotid artery to attach a silver-wire recording electrode (0.6-mm diameter) connected to a high-impedance probe. A second electrode was implanted under the skin as a reference. Action potentials were amplified with a low-noise amplifier (BIO amplifier, AD Instrument, Oxford, UK; Gain:105), band-pass filtered (100-1000 Hz), digitized (PowerLab 16/35 digitizer, AD Instrument, Oxford, UK) and acquired with the LabChart 7 software (AD Instrument, Oxford, UK). Nerve activity was analyzed with LabChart 7 and resulting data compared with 2-way nova followed by Bonferroni post-hoc tests. Glucagon was quantitated by radioimmunoassay (Linco Research Inc.) at the end of experiment in plasma prepared from blood sampled by intracardiac puncture in the presence of 1 μg/ml aprotinin and 1 mM EDTA.

Supplemental References

Berthoud, H.R., Jedrzejewska, A., and Powley, T.L. (1990). Simultaneous labeling of vagal innervation of the gut and afferent projections from the visceral forebrain with dil injected into the dorsal vagal complex in the rat. J Comp Neurol 301, 65-79.

Dani, V.S., Chang, Q., Maffei, A., Turrigiano, G.G., Jaenisch, R., and Nelson, S.B. (2005). Reduced cortical activity due to a shift in the balance between excitation and inhibition in a mouse model of Rett syndrome. Proc Natl Acad Sci U S A 102, 12560-12565.

Hille, B. (2001). Ion channels of excitable membranes. (Sunderland, MA, USA: Sinauer Associates, Inc).

Madisen, L., Mao, T., Koch, H., Zhuo, J.M., Berenyi, A., Fujisawa, S., Hsu, Y.W., Garcia, A.J., 3rd, Gu, X., Zanella, S., Kidney, J., Gu, H., Mao, Y., Hooks, B.M., Boyden, E.S., Buzsaki, G., Ramirez, J.M., Jones, A.R., Svoboda, K., Han, X., Turner, E.E., and Zeng, H. (2012). A toolbox of Cre-dependent optogenetic transgenic mice for light-induced activation and silencing. Nat Neurosci 15, 793-802.

Madisen, L., Zwingman, T.A., Sunkin, S.M., Oh, S.W., Zariwala, H.A., Gu, H., Ng, L.L., Palmiter, R.D., Hawrylycz, M.J., Jones, A.R., Lein, E.S., and Zeng, H. (2010). A robust and high-throughput Cre reporting and characterization system for the whole mouse brain. Nat Neurosci 13, 133-140.

Magnan, C., Collins, S., Berthault, M.F., Kassis, N., Vincent, M., Gilbert, M., Penicaud, L., Ktorza, A., and Assimacopoulos-Jeannet, F. (1999). Lipid infusion lowers sympathetic nervous activity and leads to increased beta-cell responsiveness to glucose. J Clin Invest 103, 413-419.

Mounien, L., Marty, N., Tarussio, D., Metref, S., Genoux, D., Preitner, F., Foretz, M., and Thorens, B. (2010). Glut2-dependent glucose-sensing controls thermoregulation by enhancing the leptin sensitivity of NPY and POMC neurons. FASEB J 24, 1747-1758.